Impact of dephasing probes on various incommensurate lattice models

A Thesis

submitted to
Indian Institute of Science Education and Research Pune
in partial fulfillment of the requirements for the
BS-MS Dual Degree Programme

by

Bishal Kumar Ghosh

Indian Institute of Science Education and Research Pune
Dr. Homi Bhabha Road,
Pashan, Pune 411008, INDIA.

May, 2023

Supervisor: Bijay Kumar Agarwalla

Certificate

This is to certify that this dissertation entitled Impact of dephasing probes on various incommensurate lattice modelstowards the partial fulfilment of the BS-MS dual degree programme at the Indian Institute of Science Education and Research, Pune represents study/work carried out by Bishal Kumar Ghosh at Indian Institute of Science Education and Research under the supervision of Bijay Kumar Agarwalla, Associate Professor, Department of Physics , during the academic year 2018-2023.

Bijay Kumar Agarwalla

Committee:
Bijay Kumar Agarwalla
Rejish Nath

This thesis is dedicated to my parents.

Declaration

I hereby declare that the matter embodied in the report entitled Impact of dephasing probes on various incommensurate lattice models, are the results of the work carried out by me at the Department of Physics, Indian Institute of Science Education and Research, Pune, under the supervision of Bijay Kumar Agarwalla and the same has not been submitted elsewhere for any other degree.

Bishal Kumar Ghosh

Acknowledgments

I am eternally grateful to Prof. Bijay Kumar Agarwalla for being a supportive supervisor. His insights and enthusiasm to have discussions on the smallest of details are what gave shape and form to the project. I am also grateful to Sandipan Mohanta and Madhumita Saha for helping me with many calculations and for having discussions with me that clarified numerous small errors that I had made. I would also like to thank Prof. Rejish Nath for providing valuable feedback on my work. I am grateful to Prof. Manas Kulkarni, with whom we collaborated for part of my thesis; discussions with him and the opportunities he provided me to visit ICTS helped me in my work. Lastly, I'll like to thank my parents and my friends, who were my constant companions during my journey as a science student.

Abstract

This thesis aims to study quantum transport and quantum dynamics properties in one dimensional quasi-periodic lattice systems. In particular we aim here to understand the impact of external probes on both the steady state and in transient. We therefore focus on two different setups: (i) a quasi-periodic lattice subjected to a chemical potential difference at its two end that drives current through the lattice and hence in a non-equilibrium steady state. We then perturb the system by a single dephasing probe and analyze the steady state transport properties. (ii) In another setup we consider a quasi-periodic lattice which is initially filled with a certain number of electrons at the central part of the lattice and is further subjected to dephasing probes at the filled sites. We then investigate the dynamics of the electron density and the scaling of the density front under two distinct scenarios: (a) when the number of probes N_p connected to the lattice chain is of the same order as the number of filled electrons N_f, and (b) when the number of probes N_p scales as $\sqrt{N_f}$.

Contents

List of Figures

Chapter 1

Introduction

The overall idea of the thesis is to understand the open quantum system. Closed systems are isolated, and the dynamics evolve through unitary dynamics. This is in contrast to a system attached to an environment where the dynamics become non-unitary. Studying this becomes relevant as the environment infers dissipative and sometimes dephasing imperfections to the system. The way we describe the influence of the environment can be critical in our understanding of the system. A simple addition of the dissipation phenomenologically could induce violations of commutation properties, and thus a systematic procedure must be undertaken. Now the effect of this can be understood in two ways, studying either the effect the environment has on the steady state of the system or taking the approach of studying how the dynamics of the system are changed on coupling with the environment.

In this thesis, we are interested in investigating quantum dynamics and also long-time non-equilibrium steady state properties of open systems that are subjected to various kinds of openness in interesting lattice systems that offer underlying rich properties. In this context, we would like to investigate a particular type of incommensurate lattice model, namely the Aubry-André-Harper (AAH) model. Such a model has interesting transitions that we will be explaining below and we would like to understand how perturbing such a system via dissipative and dephasing channels would impact the transport properties. In what follows, we first introduce the AAH lattice model and its properties and then a brief introduction to the techniques that are extensively used in this thesis.

1.1 One dimensional quasiperiodic Aubry-André-Harper lattice model (AAH)

Quasi-periodic potentials utilise functions that are nearly periodic but contain a certain degree of randomness. The Aubry-Andrè-Harper model is a relatively well-known model for realising such a system [1, 2]. The on-site potential of the Hamiltonian with the AAH model is stated as,

$$\epsilon_i = 2\lambda \cos\left(2\pi b i + \Phi\right) \tag{1.1.1}$$

The value of λ determines the onsite potential's strength; however, because b is an irrational number, it assures that the complete function never repeats along the lattice, which accounts for the potential's non-periodic nature. The phase ϕ emulates different realizations of the quasi-periodic lattice.

The properties of AAH model can be quite rich, with single particle eigenstates exhibiting localisation even in a one-dimensional model. The one-dimensional AAH model in the second quantized version can be written as

$$\hat{H} = \sum_{l=1}^{N} \left(c_{l+1}^{\dagger}\, c_l + c_l^{\dagger}\, c_{l+1} \right) + 2\lambda \sum_{l=1}^{N} \cos\left(2\pi b l\right) c_l^{\dagger}\, c_l. \tag{1.1.2}$$

Interestingly, such a model goes through a localisation transition at the critical value of $\lambda_c = 1$ [1, 2]. The single particle eigenstates remain delocalized at $\lambda < 1$ and become localized when $\lambda > 1$ [1, 2, 3, 4, 5]. This transition can be understood by observing the self-duality property of the AAH model. The self-duality arises on doing a certain transformation which is closely related to the Fourier transformation.

In this thesis, we are going to consider the above AAH model and understand the transport properties in presence of the so-called dephasing probes which will be introduced later. In order to understand the transport properties we are going to rely on two complementary approaches, namely (i) non-equilibrium Green's function (NEGF) approach and (ii) the quantum master equation (QME) approach. In what follows, we will first discuss the NEGF approach.

1.2 The Non-Equilibrium Green's function

The Non-equilibrium Green's function (NEGF) [6, 7, 8] is a convenient tool for calculating steady-state properties in nanoscale and mesoscopic scale quantum setups such as charge current and density of states. The Green's function calculates the response of the system to a constant perturbation introduced to the system, calculating the Green's function is much easier than solving the eigenvalue problem, and all the single-particle properties of the system can be found using the Non-Equilibrium Green's function.

1.2.1 Green's function for second quantized representation

Any general quadratic Hamiltonian in second quantization form can be expressed as,

$$\mathcal{H} = \sum_{i,j=1}^{N} c_i^\dagger h_{ij} c_j, \tag{1.2.1}$$

where c_i is the fermionic annihilation operator at the i-th site, $c_i^\dagger$ is the corresponding creation operator. h_{ij} is the single particle matrix elements. Below we perform a Green's function calculation by assuming the operators as bosonic in which case we have the commutation algebra between the creation and annhilation operators. Similar analysis can be trivially extended for fermionic case where the commutators are replaced by anti-commutators. We define the retarded correlator as [6, 7, 8]

$$g^r_{B,ij}(t) = -i\theta(t)\langle[c_i(t), c_j^\dagger(0)]\rangle, \quad i,j = 1, \cdots N \tag{1.2.2}$$

which translates to following differential equation as,

$$\partial_t g^r_{B,ij}(t) = -i\delta(t)\langle[c_i(t), c_j^\dagger(0)]\rangle - i\theta(t)\langle[\dot{c}_i(t), c_j^\dagger(0)]\rangle \tag{1.2.3}$$

From Heisenberg equation we know that,

$$\dot{c}_i(t) = -i[c_i(t), \mathcal{H}] \tag{1.2.4}$$

which then reduces to,

$$\begin{aligned}
-i[c_i(t), \mathcal{H}] &= -i \sum_{pq} h_{pq}[c_i, c_p^\dagger c_q] \\
&= -i \sum_{pq} h_{pq}[c_i c_p^\dagger c_q - c_p^\dagger c_q c_i] \\
&= -i \sum_{pq} h_{pq}[c_p^\dagger c_i c_q + \delta_{ip} c_q - c_p^\dagger c_q c_i] \\
&= -i \sum_{pq} h_{pq}[c_p^\dagger [c_i, c_q] + \delta_{ip} c_q] \qquad ([c_i, c_q] = 0) \\
&= -i \sum_{q} h_{iq} c_q
\end{aligned}$$

Putting this in equation (2) we get,

$$\partial_t g^r_{B,ij}(t) = -i\delta_{ij} - \sum_q h_{iq}\theta(t)\langle[c_q(t), c_j^\dagger(0)]\rangle \tag{1.2.5}$$

Now taking a Fourier transform and ensuring the causality condition we get,

$$(\omega + i0^+) g^r(\omega) = \mathbb{I} + h\, g^r(\omega)$$

$$g^r(\omega) = [(\omega + i0^+)\mathbb{I} - h]^{-1}$$

where the above equations are now in the form of matrices with $\mathbb{I}$ being the Identity matrix. All of the matrices are of $N \times N$ where N is the number of lattice sites. In a similar fashion, it can be shown that the advanced Green's function is related to retarded component by,

$$g^a(\omega) = \big[g^r(\omega)\big]^\dagger \tag{1.2.6}$$

Note the the above derivation holds true for an isolated system. However, if one has a system + bath setup and look at the retarded component of the system Green's function, it usually takes the form [6, 7, 8, 9] ,

$$G^r(\omega) = [(\omega + i0^+)\mathbb{I} - h - \Sigma^r(\omega)]^{-1} \tag{1.2.7}$$

and $G^a(\omega) = \big[G^r(\omega)\big]^\dagger$. Here $\Sigma^r(\omega)$ takes into account the effects from the bath and is called the self-energy.

1.3 Quantum Master Equations

For deriving the quantum master Equations, we start with the isolated system evolution consisting of system and a bath and then introduce the interaction picture representation to trace out the bath [10, 11, 12, 13, 14]. The isolated system evolution is governed by Liouville equation,

$$\frac{\partial \rho(t)}{\partial t} = -[H(t), \rho(t)] \tag{1.3.1}$$

Now the full Hamiltonian of a setup can be written as follows,

$$H_S = H_0 + H_I \tag{1.3.2}$$

where the H_0 is time-independent and is thus called a free Hamiltonian. Thus if we talk about the evolution of the density operator in the Schrodinger picture, it evolves as,

$$\rho(t) = U(t, t_0)\rho(t_0)U^\dagger(t, t_0) \tag{1.3.3}$$

Now when we move to the interaction picture, we can separate the unitary operator into two terms, $U(t, t_0) = U_0(t, t_0)U_I(t, t_0)$, where U_0 is the unitary operator for the free Hamiltonian, and hence we get that the expression for it as

$$U_0(t, t_0) = \exp\big[-iH_0(t - t_0)\big], \tag{1.3.4}$$

thus the observable then evolves as,

$$\langle\hat{O}(t) = \exp\big[iH_0(t - t_0)\big]\hat{O}\exp\big[-iH_0(t - t_0)\big] \tag{1.3.5}$$

Hence we see that the evolution for the observable is via the free operator rather than the interaction one.

1.3.1 System v/s Environment evolution

Now suppose S is a sub-system of a larger combined system, as shown in the diagram. We have unitary dynamics for the closed system, but effect of the environment on the system cannot be simply put as a unitary transformation. Now we will trace out the environment

to get a reduced density operator defining the system only as,

$$\rho_S(t) = tr_E \rho(t) \tag{1.3.6}$$

Thus the Hilbert system of the total system and environment can be written as a tensor product like below,

$$\mathcal{H} = \mathcal{H}_S \bigotimes \mathcal{H}_E \tag{1.3.7}$$

System Hilbert space is written as $\mathcal{H}_S$ and the environment Hilbert space as $\mathcal{H}_E$.

1.3.2 Lindbladian Quantum Master Equation

Now in the interaction picture, the total evolution is written as [11, 12, 13, 14]

$$\frac{d\hat{\rho}(t)}{dt} = -i\left[\hat{H}_I(t), \hat{\rho}(t)\right] \tag{1.3.8}$$

and the solution to this comes out to be,

$$\hat{\rho}(t) = \hat{\rho}(0) - i\int_0^t ds\left[\hat{H}_I(s), \hat{\rho}(s)\right] \tag{1.3.9}$$

Thus putting this integrand in Eq.(1.3.8) now becomes,

$$\frac{d\hat{\rho}(t)}{dt} = -i\left[\hat{H}_I(t), \hat{\rho}(0)\right] - \int_0^t ds\left[\hat{H}_I(t), [\hat{H}_I(s), \hat{\rho}(s)]\right] \tag{1.3.10}$$

And now, we take the higher-order term of this equation by repeating this step again,

$$\frac{d\hat{\rho}(t)}{dt} = -i\left[\hat{H}_I(t), \hat{\rho}(0)\right] - \int_0^t ds\left[\hat{H}_I(t), [\hat{H}_I(s), \hat{\rho}(t)]\right] + O(s^3) \tag{1.3.11}$$

Now we assume that the strength of the interaction is small enough to ignore the higher-order terms which give,

$$\frac{d\hat{\rho}(t)}{dt} = -i\left[\hat{H}_I(t), \hat{\rho}(0)\right] - \int_0^t ds\left[\hat{H}_I(t), [\hat{H}_I(s), \hat{\rho}(t)]\right] \tag{1.3.12}$$

Now in order to get the system density matrix, we trace out the environment degrees of freedom to get,

$$\frac{d\hat{\rho}_S(t)}{dt} = -i\ tr_E\left[\hat{H}_I(t), \hat{\rho}(0)\right] - \int_0^t ds\ tr_E\left[\hat{H}_I(t), [\hat{H}_I(s), \hat{\rho}(t)]\right] \tag{1.3.13}$$

Now we further make two more assumptions. the first one states that the system and environment have short-lived correlations meaning the initial density state can be written as $\hat{\rho}(0) = \rho_S(0) \otimes \rho_E(0)$, the second assumption is the Markovian approximation that assumes the system is independent of the initial preparation of the system, this reduces the equation of motion to the Redfield equation,

$$\dot{\hat{\rho}}_S(t) = -\int_0^\infty ds\ tr_E\left[\hat{H}_I(t), [\hat{H}_I(s-t), \rho_S(t) \otimes \rho_E(0)]\right] \tag{1.3.14}$$

Finally, we assume the rotating wave approximation to get,

$$\begin{aligned}\dot{\hat{\rho}}_S(t) = &-\alpha^2 \mathrm{Tr}\left[\int_0^\infty ds \hat{H}_I(t)\hat{H}_I(t-s)\hat{\rho}(t) \otimes \hat{\rho}_E(0)\right. \\ &- \int_0^\infty ds \hat{H}_I(t)\hat{\rho}(t) \otimes \hat{\rho}_E(0)\hat{H}_I(t-s) \\ &- \int_0^\infty ds \hat{H}_I(t-s)\hat{\rho}(t) \otimes \hat{\rho}_E(0)\hat{H}_I(t) \\ &\left.+ \int_0^\infty ds \hat{\rho}(t) \otimes \hat{\rho}_E(0)\hat{H}_I(t-s)\hat{H}_I(t)\right].\end{aligned} \tag{1.3.15}$$

Finally the equation simplifies to the Lindblad quantum master equation[10]

$$\dot{\hat{\rho}}_S(t) = -i\big[H_S, \rho(t)\big] + \sum_i \gamma_i\Big(L_i\rho_S L_i^\dagger + \frac{1}{2}\big\{L_i^\dagger L_i, \rho(t)\big\}\Big), \tag{1.3.16}$$

which we are going to use later.

Now that we have introduced the AAH model and the necessary tools to investigate the transport properties, in what follows, we will introduce two different kinds of setups that we focused on in this thesis.

Chapter 2

Understanding of steady-state quantum transport in the AAH model in the presence of a single dephasing Büttiker probe using the NEGF approach

In this particular work, we want to understand the transport properties in a quasi-periodic lattice in the presence of a Büttiker probe. We work at the zero temperature regime, where the Büttiker probe works as a dephasing probe. We implement the voltage probe technique, which demands zero current flow between the probe and lattice. We hope to understand how the steady state properties change in the presence of the Büttiker probe. To realise the quasi-periodic lattice, we utilise an AAH model, which has a rich phase diagram for the single-particle eigenstates. Our observation shows a universal power law scaling in the value of conductance when there is a strong probe coupling.

2.1 Model and Theory

2.1.1 Model of the quasi-periodic lattice and the coupled probe.

The system contains a one-dimensional quasiperiodic lattice chain with length N connected to two baths at its ends and a probe at site ν. The Büttiker probes are independent local

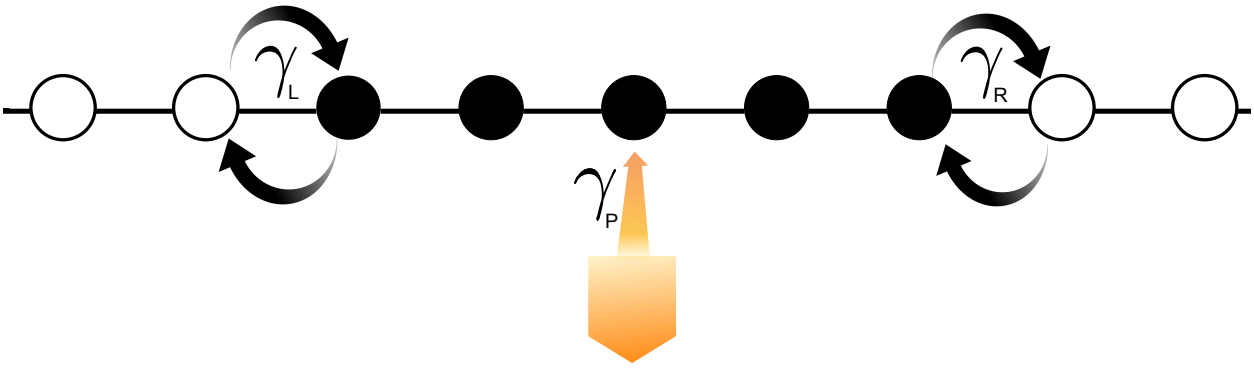

Figure 2.1: Schematic of a one-dimensional lattice chain with the first and last site attached to the left and right bath, and the central site is attached to a Buttiker probe. All the probes and baths are modelled by a semi-infinite chain. Electrons can fill into the system from the left bath with rate γ_L and from the right it can escape with rate γ_R. No net electron exchange happens between the system and the Buttiker probe.

reservoirs. The setup is modelled by the Hamiltonian given below[4],

$$H = H_S + H_B + H_{SB} + H_P + H_{PS}. \tag{2.1.1}$$

Now H_S is the system Hamiltonian which represents the quasi-periodic chain,

$$H_S = J \sum_{i=0}^{N-1} (c_{i+1}^\dagger c_i + c_i^\dagger c_{i+1}) + \sum_{i=0}^{N-1} \epsilon_i c_i^\dagger c_i \tag{2.1.2}$$

here $c_i^\dagger(c_i)$ is the creation(anhillation) operator for the electron at i^{th} site, and follow anti-commutation algebra. The two terms represent the hopping term and the on-site potential, with J representing the hopping parameter, and in our work, it is fixed to $J = 1$. Recall that the onsite potential we choose here as the AAH form given as $\epsilon_i = 2\lambda \cos[2\pi bi + \Phi]$ where b, is the golden ratio $(\sqrt{5}+1)/2$, which makes the potential quasi-periodic. Given this potential, one sees a deloalization to localization transition at value $\lambda = 1$ [1, 2, 3, 4, 15, 16].

Now in Eq. (2.1.1), the bath Hamiltonian can be written as $H_B = H_l + H_r$, and they are both modelled by a semi-infinite tight binding chain with onsite potential term ϵ_0 and hopping term J_b, respectively [4]. The coupling hamiltonian between the baths and lattice

is given by $H_{SB} = H_{Sl} + H_{Sr}$, and the coupling between the systems is given by,

$$H_{Sl} = \gamma_l r_1^\dagger c_0 + H.c. \tag{2.1.3}$$

$$H_{Sr} = \gamma_r l_1^\dagger c_N + H.c. \tag{2.1.4}$$

where both the baths are coupled to the first(last) site of the lattice chain with coupling strength $\gamma_l(\gamma_r)$. Recall that r_1 and l_1 are the annihilation operators for the right and the left bath. Now the probe connected to the ν^{th} site is also modelled as a one-dimensional tight-binding semi-infinite chain. The probe is modelled by the Hamiltonian given below [4],

$$H_p = \sum_j [\epsilon_0 d_j^\dagger d_j + t_0 d_{j+1}^\dagger d_j + H.c.] \tag{2.1.5}$$

and the Hamiltonian is coupled at the ν^{th} site by,

$$H_{PS} = \gamma c_\nu^\dagger d_{\nu 1} + H.c. \tag{2.1.6}$$

the first site of the probe will be coupled to the ν^{th} site of the lattice with a coupling strength of γ. We will now show the calculations to determine the non-equilibrium steady state conductance in the presence of a single Büttiker probe. In what follows we primarily follow the reference [4] to obtain a compact expression for steady state conductance for a single probe.

2.1.2 Non-equilibrium Green's function and the Büttiker probe approach.

Now we use the Non-equilibrium Green's function approach to calculate the important steady-state properties for the quasi-periodic lattice system[6].

As the setup is a non-interacting model and is hence fully quadratic, the charge current leaving through each α^{th} reservoir is given by the Landauer-Büttiker formula [7],

$$I_\alpha = \frac{e}{h} \sum_{\nu=1}^{N} \int_{-\infty}^{\infty} d\epsilon \mathcal{T}_{\alpha,\nu}(\epsilon)[f_\alpha(\epsilon) - f_\nu(\epsilon)], \alpha = L, R, P \tag{2.1.7}$$

Here $f_\alpha(\epsilon) = (1 + e^{\beta(\epsilon - \mu_\alpha)})^{-1}$ is the Fermi distribution function of the ω^{th} terminal with inverse temperature β and chemical potential μ_ν. $\mathcal{T}_{\alpha,\nu}$ is the transmission probability of

electrons crossing from α-th lead to ν-th lead and is computed from Green's function via the expression,

$$\mathcal{T}_{\alpha,\nu}(\epsilon) = tr[\Gamma_\alpha(\epsilon)G^r(\epsilon)\Gamma_\omega(\epsilon)G^a(\epsilon)] \tag{2.1.8}$$

here the retarded green's function G^r for the system is given by,

$$G^r(\epsilon) = [\epsilon I - H_c - \Sigma_l^r(\epsilon) - \Sigma_r^r(\epsilon) - \Sigma_p^r(\epsilon)]^{-1} \tag{2.1.9}$$

where I is the $N \times N$ identity matrix, H_c is the single particle Hamiltonian for the central system which is the quasi-periodic lattice in our case. The corrections in the retarded Green's function appear in terms of the self-energy terms associated with the baths and the probe is $\Sigma_\alpha^r(\epsilon)$ where $\alpha = L, R$ and P. As the baths are modelled as the tight-binding Hamiltonian, the self-energy term can be analytically computed and is given by [4, 17],

$$\Sigma_\alpha^r(\epsilon) = \frac{\gamma_\alpha^2}{2t_0^2}[\epsilon - i\sqrt{4t_0^2 - \epsilon^2}] \tag{2.1.10}$$

and finally $\Gamma_\alpha(\epsilon) = -2Im[\Sigma_\alpha^r(\epsilon)]$ is the spectral density. Note that $G_a(\epsilon)$ is the advanced Green's function for the setup and is related to the retarded component via by a conjugate transpose. Note that since the setup is subjected to probes, we demand that the net total particle current flowing between the probe and the system to zero, i.e. $I_P = 0$ [18, 19]. For simplicity we further set the temperature of the baths and probe to be zero . This gives us a simple effective formula for conductance.

2.2 Calculation for Conductance in non-equilibrium steady state

Following equation (2.1.7), we impose net zero charge current condition for the probe which also implies setting $I_P = 0$. This essentially fixes the local chemical potential of the probe. We then focus on close to equilibrium limit or in other words the linear-response regime and perform a Taylor expansion for the Fermi-distribution function ($f_\alpha(\epsilon)$) around the equilibrium chemical potential ϵ_F and inverse temperature β [4, 17]. We then receive,

$$f_K(\epsilon) = f_{eq}(\epsilon) - \left.\frac{\partial f_{eq}(\epsilon)}{\partial \epsilon}\right|_{\epsilon=\epsilon_F} (\mu_F - \epsilon_F) \tag{2.2.1}$$

and without loss of generality, we can assume $\epsilon_F = 0$ and evaluating $f_\mu(\epsilon) - f_\alpha(\epsilon) = -\frac{\partial f_{eq}}{\partial \epsilon}(\mu_n - \mu_\alpha)$ we get from equation (2.1.7),

$$I_P = \sum_\nu \int_{-\infty}^{\infty} \mathcal{T}_{P,\nu}[-\frac{\partial f_{eq}}{\partial \epsilon}(\mu_P - \mu_\nu)]d\epsilon = 0 \tag{2.2.2}$$

Now we expand out the summation keeping in mind that there are three terminals, the two end baths and the probe thus we get,

$$\mu_P \sum_\nu \int_{-\alpha}^{\alpha} \mathcal{T}_{P,\nu}(\frac{-\partial f_{eq}}{\partial \epsilon})d\epsilon - \nu_L \int_{-\infty}^{\infty} \mathcal{T}_{P,L}(\frac{-\partial f_{eq}}{\partial \epsilon})d\epsilon - \mu_R \int_{-\infty}^{\infty} \mathcal{T}_{P,R}(\frac{-\partial f_{eq}}{\partial \epsilon})d\epsilon = 0 \tag{2.2.3}$$

Now we expand the first term to determine the chemical potential (μ_P) of the probe.

$$\mu_P = \frac{\mu_L \int_{-\infty}^{\infty} \mathcal{T}_{P,L}(\frac{-\partial f_{eq}}{\partial \epsilon})d\epsilon + \mu_R \int_{-\infty}^{\infty} \mathcal{T}_{P,R}(\frac{-\partial f_{eq}}{\partial \epsilon})d\epsilon}{\int_{-\infty}^{\infty} (\mathcal{T}_{P,L} + \mathcal{T}_{P,R})(\frac{-\partial f_{eq}}{\partial \epsilon})d\epsilon} \tag{2.2.4}$$

Now putting this chemical potential term back in the expression for the current going to the right bath we get,

$$I_R = \frac{e}{h} \sum_\nu \int_{-\infty}^{\infty} \mathcal{T}_{R,\nu}[-\frac{\partial f_{eq}}{\partial \epsilon}(\mu_R - \mu_\nu)]d\epsilon \tag{2.2.5}$$

After which we expand the summation over the terminals,

$$\begin{aligned} I_R =& \frac{e}{h} \int_{-\infty}^{\infty} \mathcal{T}_{RL}(\epsilon)[-\frac{\partial f_{eq}}{\partial \epsilon}(\mu_R - \mu_L)] + \\ & \frac{e}{h} \int_{-\infty}^{\infty} \mathcal{T}_{R,P}(\epsilon)[-\frac{\partial f_{eq}}{\partial \epsilon}(\mu_R - \frac{\mu_L \int_{-\infty}^{\infty} \mathcal{T}_{P,L}(\frac{-\partial f_{eq}}{\partial \epsilon})d\epsilon + \mu_R \int_{-\infty}^{\infty} \mathcal{T}_{P,R}(\frac{-\partial f_{eq}}{\partial \epsilon})d\epsilon}{\int_{-\infty}^{\infty} (\mathcal{T}_{P,L} + \mathcal{T}_{P,R})(\frac{-\partial f_{eq}}{\partial \epsilon})d\epsilon})] \end{aligned} \tag{2.2.6}$$

Now in the zero temperature limit, ($\beta \longrightarrow \infty$), the derivative term becomes a delta function around ϵ_F

$$\frac{\partial f_{eq}}{\partial \epsilon} = -\delta(\epsilon - \epsilon_F), \tag{2.2.7}$$

and now solving the integrated, we get,

$$I_R = \frac{e}{h} \mathcal{T}_{RL}(\epsilon_F)[(\mu_R - \mu_L)] + \frac{e}{h} \mathcal{T}_{Rn}(\epsilon_F)[(\mu_R - \frac{\mu_L \mathcal{T}_{n,L}(\epsilon_F) + \mu_R \mathcal{T}_{n,R}(\epsilon_F)}{\mathcal{T}_{n,L}(\epsilon_F) + \mathcal{T}_{n,R}(\epsilon_F)}] \tag{2.2.8}$$

Now we can calculate the conductance ($G = I_R/\Delta V$) and knowing that $\Delta V = (\mu_R - \mu_L)$, we get

$$G = G_o\Big[\mathcal{T}_{RL}(\epsilon_F) + \frac{\mathcal{T}_{Rn}(\epsilon_F)\mathcal{T}_{nL}(\epsilon_F)}{\mathcal{T}_{Rn} + (\epsilon_F)\mathcal{T}_{nL}(\epsilon_F)}\Big]. \tag{2.2.9}$$

Hence $G_0 = e^2/h$ is the universal quantized conductance. Therefore what we finally see is that due to the presence of a single probe, the effective conductance of the system gets an additional term which interestingly seems like a Harmonic mean of the bath probe and probe-bath transmission function. In what follows we will show the numerical results for AAH model. Note that the effect of the quasi-periodic nature of the potential is buried into the Green's function through H_s and as a result in the transmission function.

2.3 Result

Now in our model, we have set up our system with a single probe attached to the central site and the baths connected to the end site, after which we have calculated eq.(2.2.9). This gives the value of the conductance as a function of the fermi energy, ϵ_F, now the band edges for the system is decided by the AAH model, which is $\epsilon_F = \pm 2$. We have produced the results for the tight-binding limit of the AAH model and the three phases of the AAH model. We have also selected lattices of three different sizes.

2.3.1 Results for the tight-binding limit.

We can see the conductance for the tight-binding model for various strengths of the Büttiker probe, a few things to notice are that the conductance has an oscillatory signature, and the conductance for Fermi energy away from the band edges keeps decreasing prominently for the large system size array. We can see that the conductances for the probe strengths less than 1.0 do not change up a lot as we approach the large size limit, but conductance decreases drastically when probe strength is above 1.0; this happens because above this limit, the probe strength becomes comparable to the hopping parameter, and thus the competing affects between them end up showing the probes influence in these strength ranges. In the next section, we will report the results for the AAH model and see how it differs from the clean chain model.

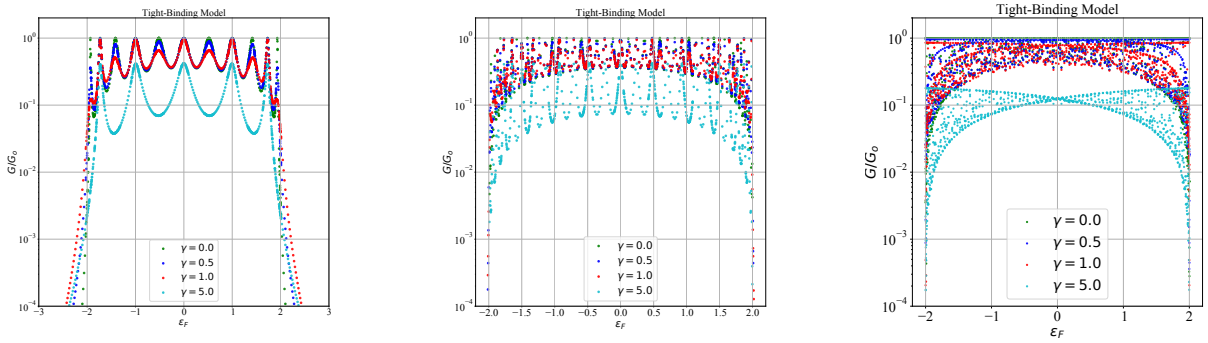

(a) 11 sites (b) 51 sites (c) 201 sites

Figure 2.2: Steady state conductance for tight-binding limit as a function of the fermi energy(ϵ_f) for three different lattice sizes. The conductance decrease becomes more and more prominent with increasing system sizes; we also see an oscillatory behaviour of the conductances with various Fermi energies, this is influenced by the probe energy levels possibly resonating with the ones in the lattice and thus increasing the conductance.

2.3.2 Results for the AAH model.

A Conductance as a function of Fermi energy for a lattice of size 201.

In the AAH model, we take three different values of λ, which belong to three different phases, i.e. the extended phase ($\lambda = 0.5$), the critical phase ($\lambda = 1.0$), and the localized phase ($\lambda = 1.2$), we then use the AAH equation ($2\lambda\cos[2\pi bi + \Phi]$) to determine the onsite potential of the lattice, and we fix $\Phi = 0.0$ and b as the golden ratio. We plot the conductance for the various energies that lie within the energy band of the AAH model; firstly, for the no-probe conductance figure, we observe that there are gaps in the energy band, which is a signature of the AAH model, and the presence of probes doesn't induce any finite conductance in these regions, secondly. The conductance values within the regions where finite conductance is already present in the absence of a probe have a roughly monotonic decrease with increased probe strength. This signature is significantly prominent in the delocalized regime, where the gaped regions are less. The conductance for the critical case has only a discrete set of values for conductance; the gaped region increases further here, And we can see that the no probe conductance also shows a huge variation in the order of magnitude; this is because now the system becomes more sensitive to the Fermi energy levels, and only some of the electron with Fermi energies around the eigenvalue of the central system can move from the left to right bath and contribute to the conductance of the system. In the next section, we discuss if the single probe results are affected by the site of attachment of the probe.

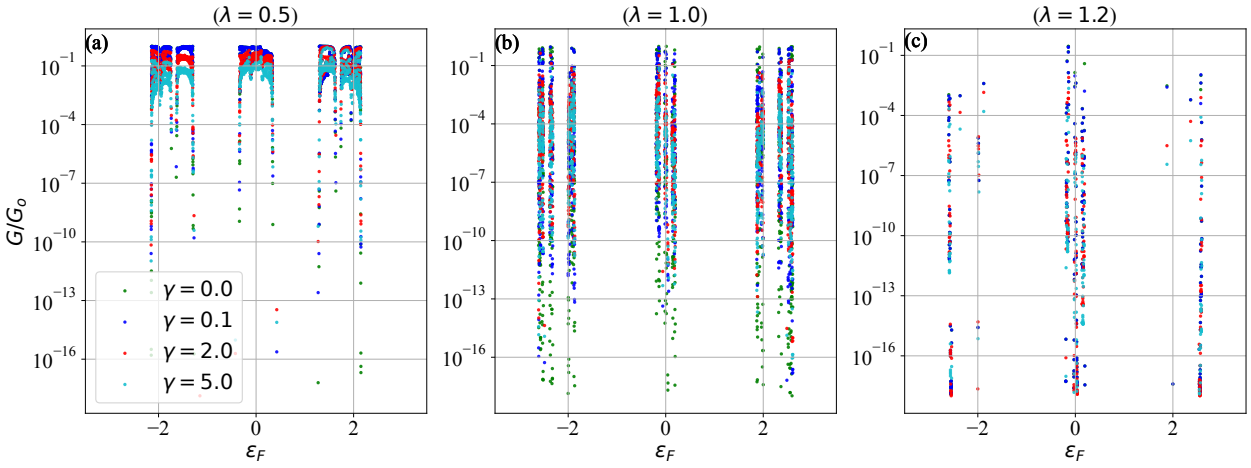

Figure 2.3: Conductance v/s Fermi-energy plot for the three phases in AAH. (a) The delocalized phase has a prominent conductance over the entire band. (b) The critical region has a lot of band gaps and also a non-monotonous behaviour in the regions with a finite probe-free conductance. (c) The localized regime has a very subdued conductance which is also understandable as the localized eigenstates would hinder any form of transport over the lattice. All the conductances are calculated in the system size of 201 with the probe connected to the central site. γ here signifies the probe strength.

B Conductance dependence on site of attachment of probe

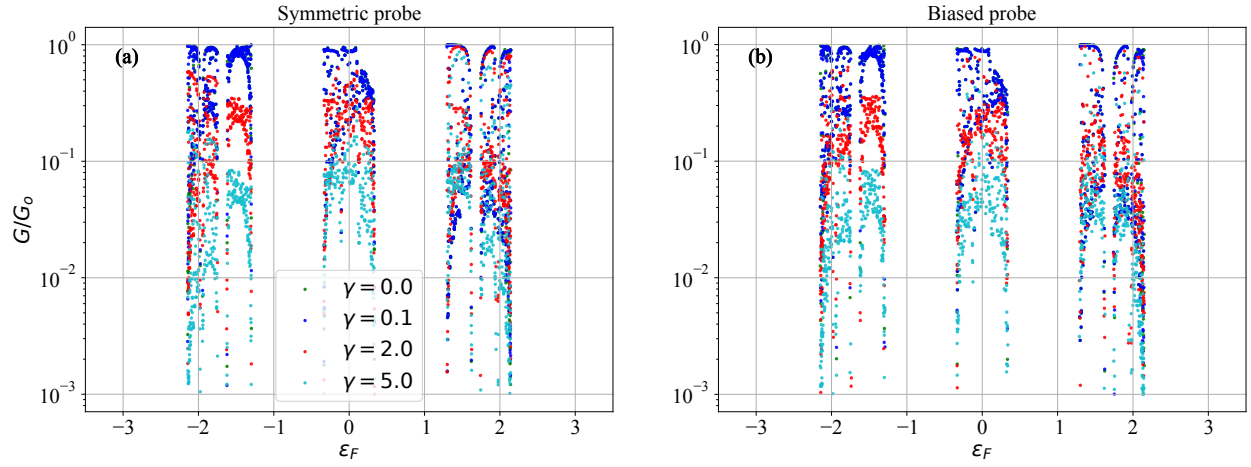

Figure 2.4: Conductance v/s Fermi-energy plot for the extended case comparing an (a)symmetric and a (b)biased probe position, both the systems have a size of 201, with the biased setting having the probe attached at site 50 and the symmetric setting with the probe attached at site 100(symmetrically central position).

We have another plot fig(2.4) above comparing the two cases of the probe connected to a symmetric and asymmetric lattice site. The symmetric probe is attached at the exact central site in the 201-length lattice, and the asymmetric probe is attached such that there is a bias in the distance between the probe and the baths. It's kept at position 50 with a 201 lattice size. We observe that even though there might be a bias in the transmission values between the right bath and the probe and also the probe and left bath, the conductance profile remains independent of that. Moreover, for the quasi-periodic lattice, we have chosen the value of λ to be 0.5, as we are working in the delocalized regime; hence the strength of the quasi-periodic lattice is not so high, thus the on-site potential between the central site and the biased site would not significantly differ. Thus the single probe conductance has the same features for both settings.

C Study of finite size effects on the steady-state conductance features.

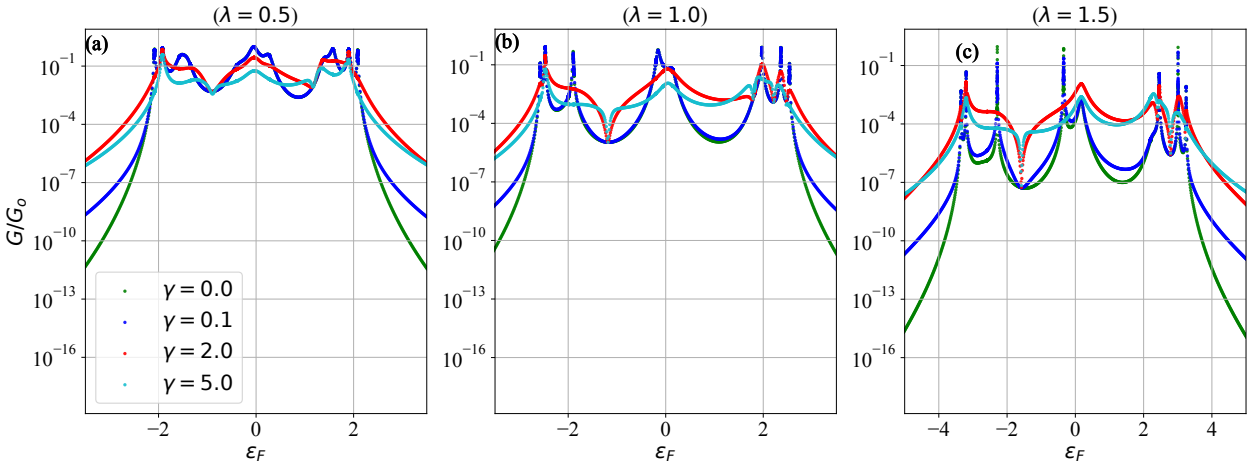

Figure 2.5: Conductance v/s Fermi-energy plot for lattice size of 11, we see that the probe induces certain conductance for the band gap regimes also.

To understand the effects of the Büttiker probe, we further study how the conductance of the model changes when we have the single probe connected to a smaller-sized lattice. This boosts the effect that the probe might have on the conductance of the lattice as now the effect of the probe shifts towards a more extensive case. The results for the 11 site case are shown in fig(2.5), and the first thing to notice is that there is now finite conductance in the entire band spectrum of the lattice. The probe can enhance the conductance in regions beyond the band edges of the central system (finite conductance at $\epsilon_F < 2$ and $\epsilon_F > 2$). The

band gaps that were present in the large lattice limit for the AAH case now have a finite conductance in the absence of the probe. A peculiar feature to note in the 11-site case is the crossover in the monotonous nature of the conductance with increasing probe strength. The previous fig(2.4) for the conductance when 201 sites are present showed a decrease in conductance throughout the spectrum but in the small lattice case, there are regimes where the conductance is enhanced due to the Büttiker probe, especially in the regions where there is an AAH band gap. Moreover, even in the localized regime, there is now significant conductance.

For the lattice size of 51 (fig(2.6)) also, we observe that the probe enhances conductance along the AAH band gaps, but in this case, the band edges of the AAH become much more prominent as there is not a significant conductance for $\epsilon_F < -2$ and $\epsilon_F > 2$. The increase in conductance is also not monotonous, and we see that the conductance for probe strength of $\gamma = 2.0$ and $\gamma = 5.0$ nearly coincide. Through this analysis, we have figured out that the probe has very non-trivial effects on the steady-state conductance; thus, to analyze this further, we select certain values of ϵ_F and plot the conductance as a function of the probe strength.

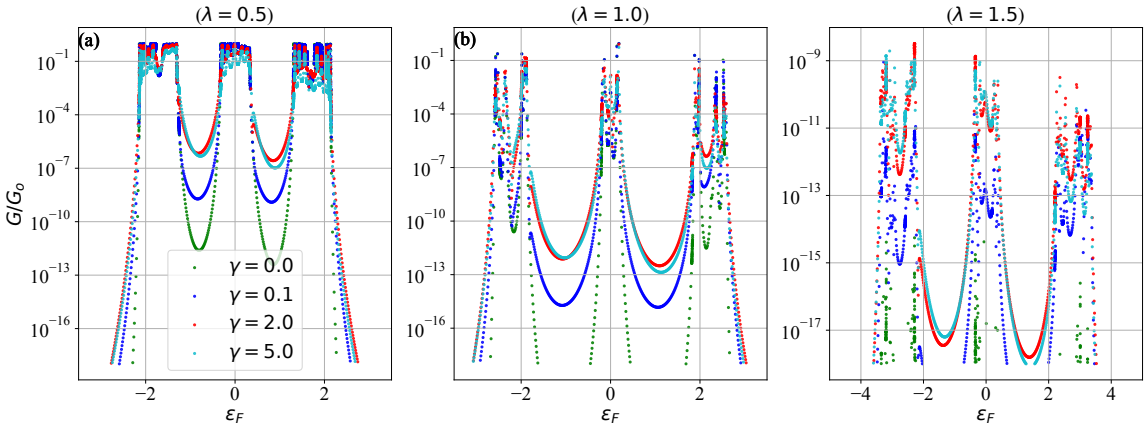

Figure 2.6: Conductance v/s Fermi-energy plot for lattice size of 51, we see that the probe induces certain conductance for the band gap regimes also, but the peculiar conductance is no longer seen.

2.3.3 Conductance scaling with probe strength

In the setup with 201 sites and a single Büttiker probe, we try to see how the conductance scales with the conductance (fig(2.7)); a few observations we can make are that the conduc-

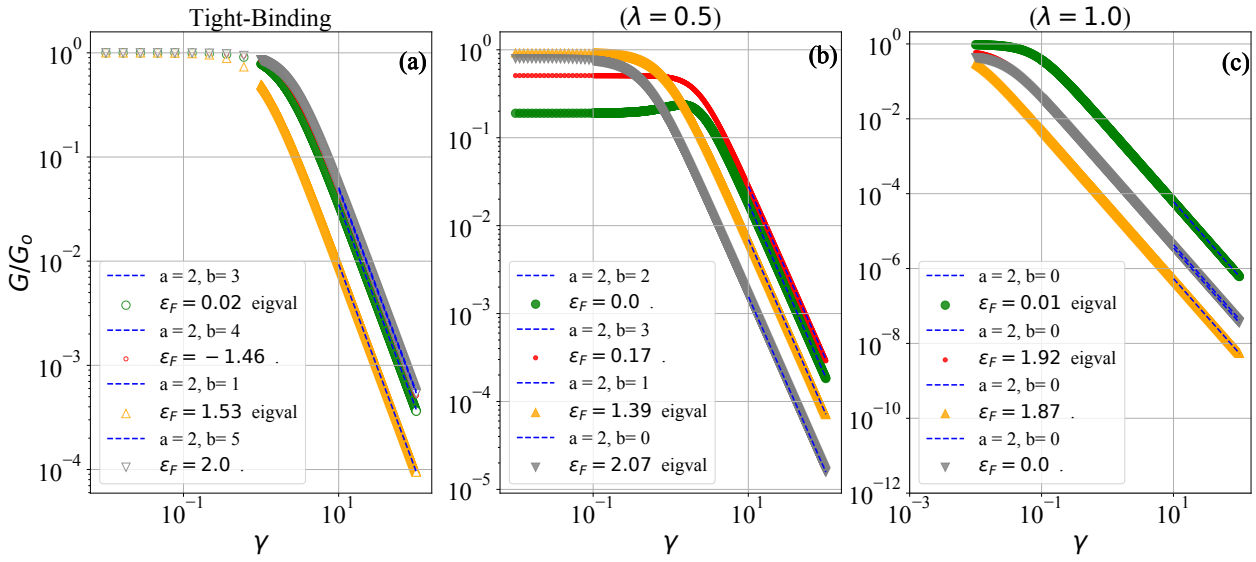

Figure 2.7: Plot for non-equilibrium steady state conductance as a function of the probe strength in a log-log scale with the lattice size of 201 and the underlying Hamiltonian with (a)tight-binding, (b)Delocalized AAH and (c)Critical AAH model. The legend shows whether the Fermi energies(ϵ_f) belong to the eigenvalue of the AAH lattice or not. We are fitting the b/γ^a curve.

tance remains nearly invariant when the probe strength is an order of magnitude below the hopping strength. For the delocalized regime, when the probe strength becomes comparable to the magnitude of the hopping parameter, we observe that depending on the Fermi energy, there is either an enhancement in the conductance. This is particularly seen for the Fermi energy of $\epsilon_F = 0$. We also observe that there is a monotonous decrease of the conductance for the strength of γ greater than a critical value. The critical value is smaller for the Fermi energies belonging to the side bands than the central band of the delocalized AAH regime. We then do a curve fitting for the equation 'b $\times \frac{1}{\gamma_p^a}$' for the regions where the conductance becomes monotonously decreasing to find that the conductance decays as a power law $1/\gamma^2$. This feature is also observed in the tight-binding limit, except that the crossover to a monotonously decreasing function is independent of the Fermi energy. Finally, the universal scaling of the conductance also shows up for the critical case of AAH, but the crossover, in this case, occurs for a very small probe strength, and the invariance in conductance for the critical case does not show up at least for the probe strengths we have reported. To understand the crossover much better, we plot the same plots in a linear-log scale (fig(2.8)). The crossover can be clearly seen by observing the critical value of the probe

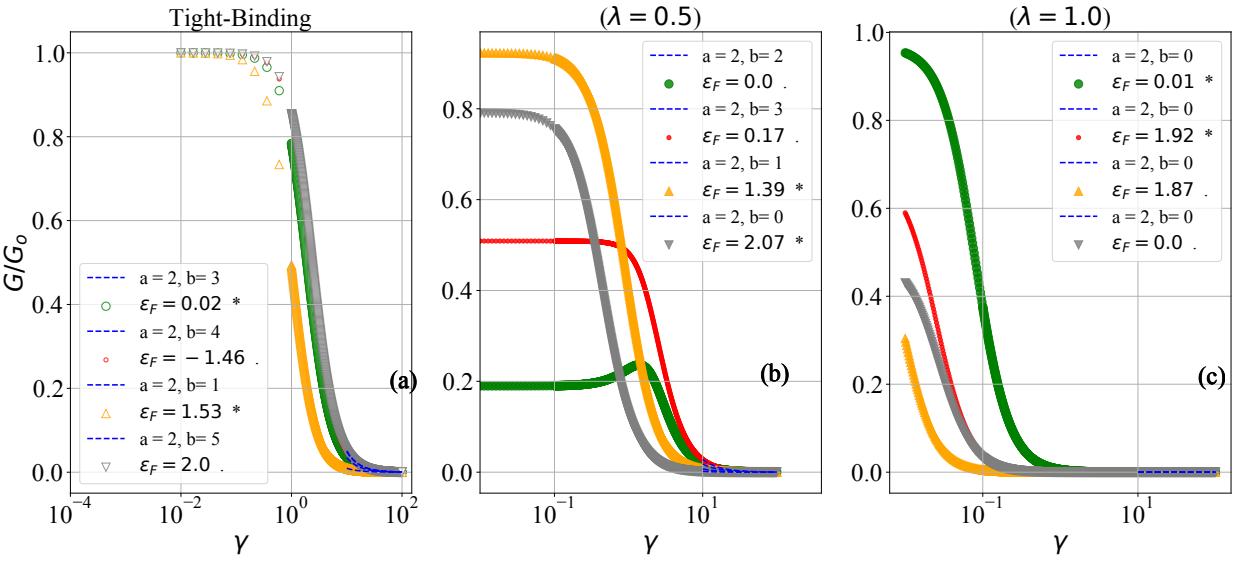

Figure 2.8: Plot for non-equilibrium steady state conductance as a function of the probe strength in a log-linear scale with the lattice size of 201 and the underlying Hamiltonian with (a)tight-binding, (b)Delocalized AAH and (c)Critical AAH model. The legend shows whether the Fermi energies (ϵ_F) belong to the eigenvalue of the AAH lattice or not. We are fitting the b/γ^a curve. The crossover region can be identified by observing the value for which the conductance suddenly drops to a very small but finite value.

strength where the conductance suddenly decreases, as in the log-log scale; that would be the point when the conductance departs from the nearly invariant value. From this plot, we observe that the crossover to the power law arrives much faster in the critical case than in the delocalized case; moreover, for the delocalized case, there is a separation depending on the Fermi energy being probed.

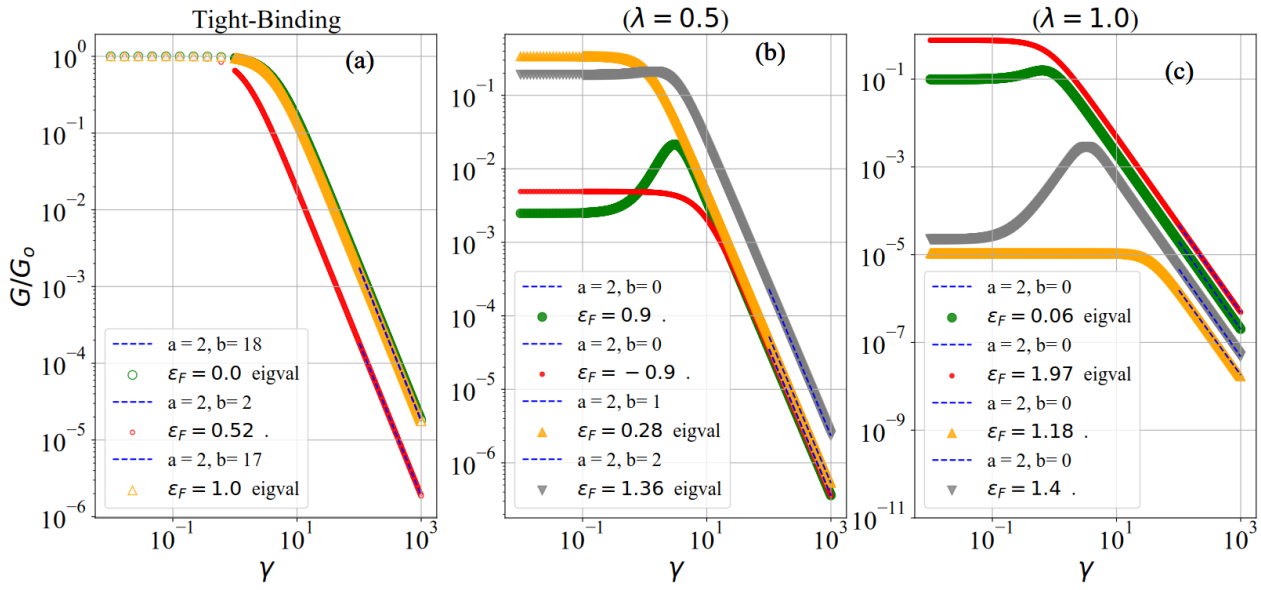

Figure 2.9: Plot for non-equilibrium steady state conductance as a function of the probe strength in a log-log scale with the lattice size of 11 and the underlying Hamiltonian with (a)tight-binding, (b)Delocalized AAH and (c)Critical AAH model. The legend shows whether the Fermi energies (ϵ_F) belong to the eigenvalue of the AAH lattice or not. We are fitting the b/γ^a curve. We can observe that the conductance enhances for particular values of Fermi energy (ϵ_F) in the AAH model.

In figure (2.9), we now try to study how the finite size affects the conductance scaling as a function of the probe strength; now we use two different types of Fermi energy, one type where the Fermi energy belongs to the AAH band gap and the other where the Fermi energy is one of the eigenvalues of the system. We observe that for the Fermi energy belonging to the AAH band gap, the conductance is significantly enhanced, as can be seen for $epsilon_f = 0.9$ in the delocalized case. The same enhanced conductance feature also shows up for the critical case, where again, picking up a Fermi energy from the band gap shows an enhancement in the conductance with the probe. Although despite the enhancement in the conductance for probe strength $\gamma \sim 1.0$, the power law scaling of the probe still shows up for the higher probe strength, and even in this case, the power law is $1/\gamma^2$

2.4 Summary and outlook

In summary, we have investigated the effect of a single dephasing Büttiker probe on the steady-state transport properties of a quasi-periodic lattice. The conductance calculated from the NEGF approach shows a universal power law decay with the probe strength. Interestingly, we observe that the power law decay is universal across the tight-binding and the AAH model. Moreover, there is an enhancement in conductance for the no-transport regions of the AAH model when we have a small lattice; thus finite size effect helps enhance the transport in the presence of the Büttiker probe. As a future problems we can investigate how to find the power law scaling for the strong γ limit analytically using the NEGF approach. Another interesting problem would be to investigate how the probe number scaling from a single probe to an extensive case affects the power law. In the next chapter, we consider a different setup that includes dephasing probe and study quantum dynamics.

Chapter 3

Study of quantum dynamics in AAH model in the presence of single and multiple dephasing probe using the quantum master equation approach

In this work, we consider a one-dimensional incommensurate lattice model that offers various kinds of single-particle states, with a certain filling of electrons N_f and the electrons are further connected to external probes at that point N_p. The schematic for the setup is given in Fig(??).

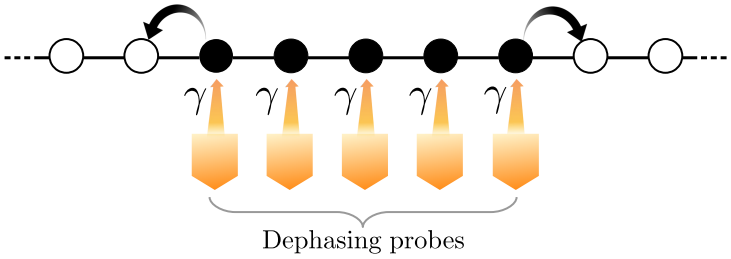

Figure 3.1: Schematic of a fermionic one-dimensional lattice chain with a certain part of the lattice is initially filled with electrons which are represented here by filled circles. The other lattice sites are empty. At the filled lattice sites, additional dephasing probes are attached with coupling strength γ.

We focus on the dynamics of the local density profile and the scaling of the density front with time. We identify two distinct regimes: (i) the density front that evolves in the regime

where probes are absent which we henceforth refer to as the outer regime and (ii) the density front that evolves in the regime where probes are present, henceforth referred to as the inner regime.

The work is organized as follows: In Sec. 3.1, we first discuss the model by writing down the Hamiltonian of the lattice and the Lindblad master equation to mimic the dephasing probes. We then provide the details about obtaining the time evolution equation for single-time two-point correlation functions that control the dynamics of the local density profile. Followed by section 3.2 where the results showing the phase co-existence in different modes are discussed. We then follow it up with the discussion on the coherence matrix, thus providing a foundation on how the dephasing probe is working.

3.1 Model and Method

In this work, we are interested in understanding the quantum dynamics of an initially filled lattice in presence of dephasing probes. To understand transport properties under various phases, we focus on a class of incommensurate lattice models that are subjected to dephasing probes. We write down the Hamiltonian for the lattice as

$$\hat{H}_S = \sum_{i=1}^{N} \epsilon_i \, c_i^\dagger \, c_i + \sum_{i=1}^{N} J \left(c_{i+1}^\dagger \, c_i + c_i^\dagger \, c_{i+1} \right). \tag{3.1.1}$$

Here $c_i^\dagger$ and c_i are the creation and the annihilation operators for an electron at a particular site i. The first term represents the onsite the second term is the hopping term, with J as the hopping parameter. The quasi-periodicity comes to form the on-site potential ϵ_i which for the Aubry-André-Harper model (AAH) is,

$$\epsilon_i = 2\,\lambda \, \cos[2\pi b i + \Phi]. \tag{3.1.2}$$

Here λ is the strength of the potential, b is an irrational number that makes the potential quasi-periodic. For our work, we have taken the value of b to be $(1+\sqrt{2})/5$, and Φ is the phase factor that generates the different configurations for the quasi-periodic potential. The λ values signify the strength of the quasi-periodic potential, with the value of $\lambda < 1$ making all the delocalized states, and the single-particle states become localized when we take the parameter $\lambda > 1$. The exact value of $\lambda = 1$ takes us to the critical phase, which is neither localized nor delocalized.

As mentioned before, in order to implement the dephasing probes, we model the dynamics of the lattice chain via a Lindblad quantum master equation given by[10, 20],

$$\dot{\hat{\rho}}_S = -i\big[H_S, \rho_S\big] + \sum_{i=1}^{N_p} \gamma_i \Big(L_i \rho_S L_i^\dagger + \frac{1}{2}\big\{ L_i^\dagger L_i, \rho_S \big\} \Big) \tag{3.1.3}$$

where ρ_S is the reduced density operator for the system (the lattice chain). Each jump operator L_i representing dephasing, $L_i = \hat{n}_i = \hat{c}_i^\dagger \hat{c}_i$ which is a Hermitian operator[20]. Here, γ_i mimics the probe coupling strength. In our study, we focus on the setup, we have used an extensive number of probes, with the number of probes (N_p) being equal to the number of initially filled sites (N_f). Now to study the dynamics initiated by the probe, we will try to see how the correlation matrix is affected when the probe is coupled. In the absence of the probe, the unitary dynamics make the correlation matrix gain off-diagonal elements, i.e. the system picks up quantum coherences. This, in turn, drives the unitary dynamics, which will further drive the density front. Thus the evolution of the two-point correlator now becomes[20, 21],

$$\begin{aligned} \frac{d}{dt}\langle \hat{c}_i^\dagger \hat{c}_j \rangle &= i\Big(\langle \hat{c}_{i+1}^\dagger \hat{c}_j \rangle + \langle \hat{c}_{i-1}^\dagger \hat{c}_j \rangle - \langle \hat{c}_i^\dagger \hat{c}_{j-1} \rangle - \langle \hat{c}_i^\dagger \hat{c}_{j+1} \rangle \Big) \\ &\quad - \frac{\gamma}{2} \sum_{l=1}^{N_p} \Big(\delta_{il} \langle \hat{c}_i^\dagger \hat{c}_j \rangle + \delta_{jl} \langle \hat{c}_i^\dagger \hat{c}_j \rangle \Big) + \gamma \sum_{l=1}^{N_p} \delta_{li}\, \delta_{lj} \langle \hat{c}_l^\dagger \hat{c}_l \rangle. \end{aligned} \tag{3.1.4}$$

It is important to note that even though the master equation involves local quartic type interaction through the dissipative term, the Lindblad being Hermitian in nature, helps to close the equation of motion for two-point correlation function and doesn't involve any higher-order correlation function terms[22]. Defining $\langle \hat{c}_i^\dagger \hat{c}_j \rangle = C_{ij}$, and

$$\begin{aligned} D_{x,y} &= \frac{\gamma}{2} \sum_{i=0}^{n} \delta_{xi} \delta_{yi} \\ P_{x,y} &= \gamma \sum_{i=0}^{n} \delta_{ix} \delta_{iy} \langle \hat{c}_i^\dagger \hat{c}_i \rangle \end{aligned} \tag{3.1.5}$$

which are diagonal matrices. Note that, D captures the effect due to all the probes attached[23, 24, 25]. Putting these in we get that the equation becomes,

$$\frac{dC_{x,y}}{dt} = -i\big[H_S, C_{x,y}\big] - \sum_k \Big(C_{x,k} D_{k,y} + D_{x,k} C_{k,y} \Big) + P_{x,y} \tag{3.1.6}$$

where dimension of all the above matrices is $N \times N$ where recall that N is the number of lattice sites. Alternatively, we can express the above equation in a matrix form as,

$$\frac{d}{dt}C = -i\Big[H_S, C\Big] - \Big\{C, D\Big\} + P \tag{3.1.7}$$

which we can alternatively write as

$$\frac{d}{dt}C = -iH_eC + iCH_e^\dagger + P \tag{3.1.8}$$

where we define the effective non-Hermitian Hamiltonian $H_e = H_S - iD$ [23, 24, 25]. Equation 3.1.8 is the central equation that we use to investigate the spread of the local density profile we can see how the density front evolution takes place in real space. This is achieved via a Runge-Kutta 4th order integrator to numerically solve the above equation and obtain the density profile[26, 27]. We provide the pseudo-code for the same below, Note that we focus

Algorithm 1 Calculate $C_{x,y}(t+N*dt)$ from $C_{x,y}(t)$ using Runge-Kutta 4th order integrator

Require: initial time : t, final time : $t + N * dt$, initial two-point correlator : $C_{x,y}(t)$
  while $t <$ final time **do**
    $K_1 = dt * (-iH_eC(t) + iC(t)H_e^\dagger + P(t))$
    $K_2 = dt * (-iH_e[C(t) + K_1/2] + i[C(t) + K_1/2]H_e^\dagger + [P(C(t) + K_1/2)])$
    $K_3 = dt * (-iH_e[C(t) + K_2/2] + i[C(t) + K_2/2]H_e^\dagger + [P(C(t) + K_2/2)])$
    $K_4 = dt * (-iH_e[C(t) + K_3] + i[C(t) + K_3]H_e^\dagger + [P(C(t) + K_3)])$
    $C(t) = C(t) + (K_1 + 2K_2 + 2K_3 + K_4)/6$
  end while
  Result $= C_{x,y}(t + N * dt)$

on the situation where at the centre part of the system, there are d probes to the left and d probes to the right. We focus on cases when d is the order of the initial lattice filling. Because of this scenario, we can realise multiple phases in the system, and the extensive dephasing probe takes the dynamics to diffusive time scales.

3.2 Results

3.2.1 Results for AAH for single probe case

In this subsection, we first provide numerical findings for AAH model when it is subjected to a single dephasing probe.

A Central lattices filled

We now load the particles in the central sites and then observe the evolution. We take a 401-sized lattice with an initial filling in the central 60 sites. There is an open boundary on the lattice edges, but a large system size ensures that the boundary effects do not play any role in the dynamics. To highlight the effects of the probe in contrast to the unitary evolution, we provide the results of two simulations, one with no probe and the other with a central probe. Now due to the imbalance of fermions in the lattice sites, there is a unitary dynamics which is kick-started. And we see the initiation of an electron density wave from the sites ± 30. Now as the electrons leave the central packet, there is a similar wave created that moves inwards. Now both the waves move with the same velocity, and the dynamics remain exact in both cases, with and without a probe, until the time that the central lattice is excited, after which there is a departure of the probe case. The probe tries to pump energy into the system and, as a result, pushes down the central site away from the unitary state. In

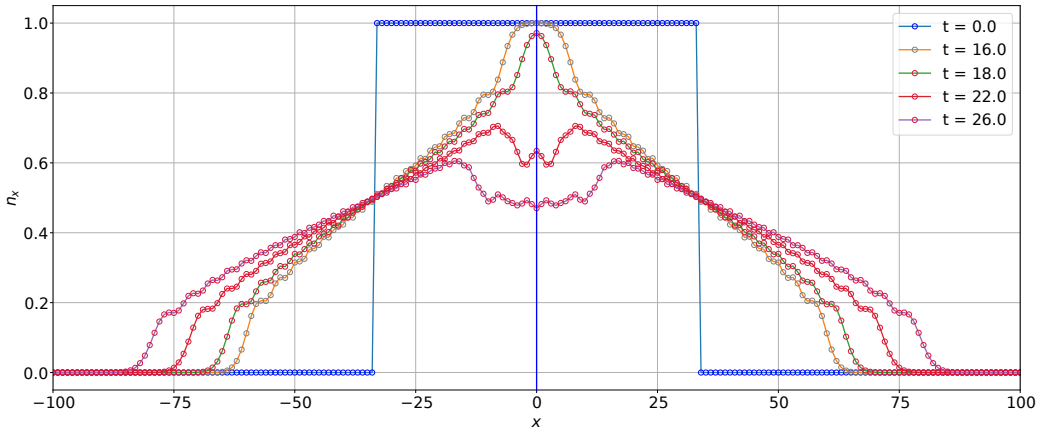

Figure 3.2: Here, we start off with loading only the central site; hence there is an inhomogeneous filling, unitary dynamics allows the system to evolve towards a homogeneous state, and we see that the central site is not changed at all in this case. The system size is 401, and hence the boundaries are very far away from the central loading. Only 60 sites are filled in this case in this case, and the lattice is in the delocalized AAH phase.

fig(3.2), we see how the unitary dynamics have made the central density packet evolve. with the central lattice sites trying to equilibrate around an average value. In fig(3.2), we see how that the unitary dynamics evolves the system till time $t = 18$, after which the central site will also have coherences generated; this allows the dephasing probe to kill these coherences

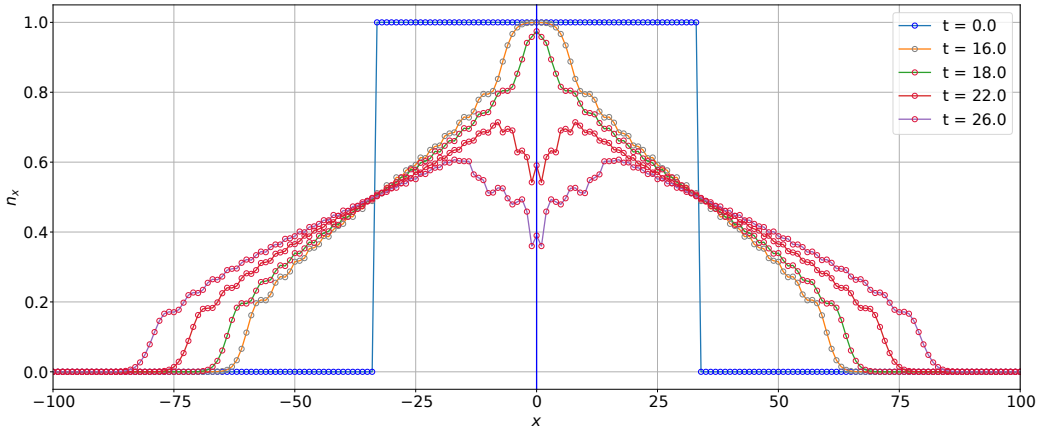

Figure 3.3: Here, we start off with loading only the central site hence there is an inhomogeneous filling. Unitary dynamics allow the system to evolve towards a homogeneous state, and we see that the central site probe gets activated at time $t = 18$. The system size is 401, and hence the boundaries are very far away from the central loading; only 60 sites are filled in this case in this case, and the lattice is clean. We can observe that the probe has now changed the central sites away from an equilibrium state. The probe strength is $\gamma = J = 1.0$.

now, thus after this point the dynamics between both the cases significantly depart from each other. In fig(3.4), we now overlay both the plots to see that there is dephasing probe dynamics which is initiated after some time, and this wave changes not only the central site dynamics but also the dynamics away from the central site.

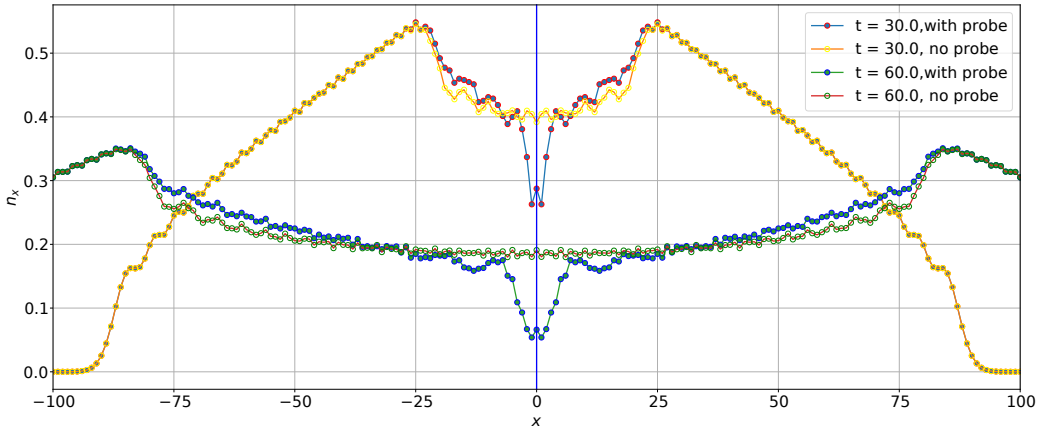

Figure 3.4: Comparative plot to show how the de-phasing probe creates the density front and how it moves forward in the clean chain. The system size is 2001, and hence the boundaries are very far away from the central loading only 1/30 sites are filled in this case in this case, and the lattice is clean. The probe strength is $\gamma = J = 1.0$

3.2.2 Results for AAH for multiple probe case

In this section, we provide our numerical findings for the AAH model. We consider the situation where given a lattice size N, we initially fill the lattice sites up to N_f and to these same sites, we connect the probes thus $N_f = N_p$.

3.2.3 AAH model- Delocalized phase $\lambda < 1$

We take $\lambda = 0.5$, [Eq.3.1.2]. The lattice size is taken to be $N = 501$, with the total number of initially filled sites (N_f) being 101, placed around the central site; this is taken so that within the time scales of consideration, the density front does not crash into the boundary. The probe number(N_p) is extensive, and hence there are 101 probes placed around the central site, placed in the positions where the initial filling of lattices is also present. We find that the outer regime scales as t, proving ballistic dynamics. Moreover, even after averaging over a hundred Φ realisations, we still observe an oscillatory feature, a signature of quantum coherence. The inner front, on the other hand, is completely diffusive as it shows that the front has collapsed on scaling by $\sqrt{t}$

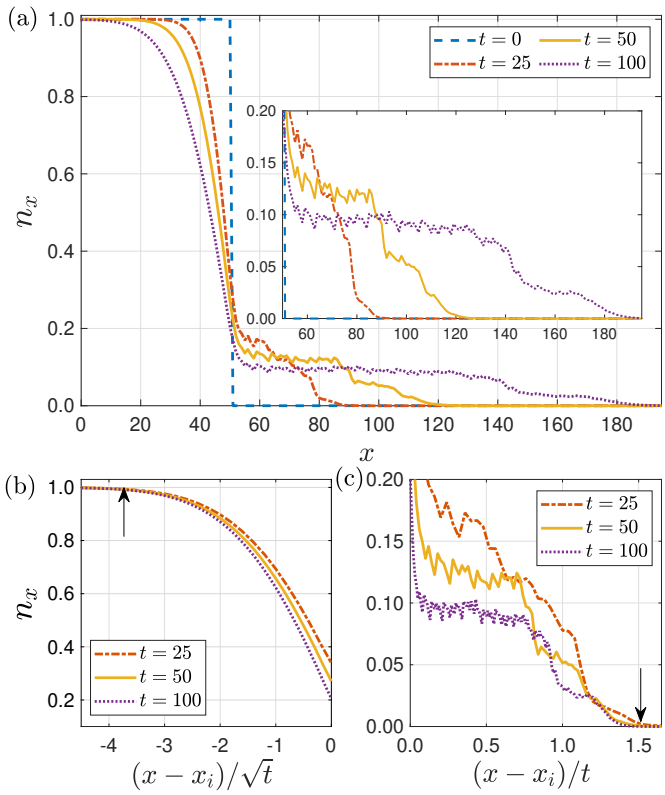

Figure 3.5: (a) Plot for density profile $n_x(t)$ as a function of x for different time snapshots for AAH lattice in the delocalized phase. The inset shows the zoomed version of the density front and to further demonstrates the site till which the density front has reached. (b) Density profile in the inner regime (sites with probe attached), and (c) density profile for the outer regime.

3.2.4 AAH model- Critical phase $\lambda = 1$

We take $\lambda = 1.0$, [Eq.3.1.2]. The lattice size is taken to be $N = 601$, with the total number of initially filled sites (N_f) being 121, placed around the central site. The probe number(N_p) is extensive, and hence there are 121 probes placed around the central site, placed in the positions where the initial filling of lattices is also present. We find that the outer regime now also scales as $\sqrt{t}$, showing diffusive dynamics, this is different from the dynamics due to the probe as it is coming as a feature of the underlying lattice being in the critical state. Moreover, even after averaging over a hundred Φ realisations, we still observe an oscillatory feature, a signature of quantum coherence. The inner front also is completely diffusive as it shows that the front has collapsed on scaling by $\sqrt{t}$. The difference between both the fronts

also shows up due to the spread of the fronts. We can see that the inner front evolves faster.

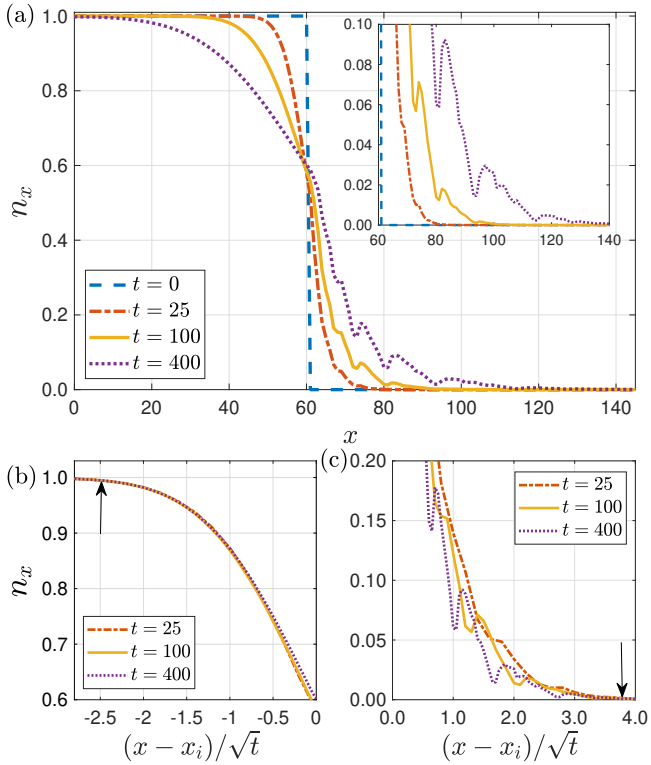

Figure 3.6: (a) Plot for density profile $n_x(t)$ as a function of x for different time snapshots for AAH lattice in the critical phase. The inset shows the zoomed version of the density front and to further demonstrates the site till which the density front has reached. (b) Density profile in the outer regime (sites with no probes), and (c) density profile for the outer regime.

3.2.5 AAH model- Localized phase $\lambda < 1$

We take $\lambda = 1.1$, [Eq.3.1.2]. The lattice size is taken to be $N = 501$, with the total number of initially filled sites (N_f) being 301, placed around the central site. The probe number(N_p) is extensive, and hence there are 301 probes placed around the central site, placed in the positions where the initial filling of lattices is also present. We find that the outer regime scales as $\log t$, proving localized dynamics. Moreover, even after averaging over a hundred Φ realisations, we still observe an oscillatory feature which is a signature of quantum coherence. The inner front on the other hand is completely diffusive as it shows that the front has collapsed on scaling by $\sqrt{t}$

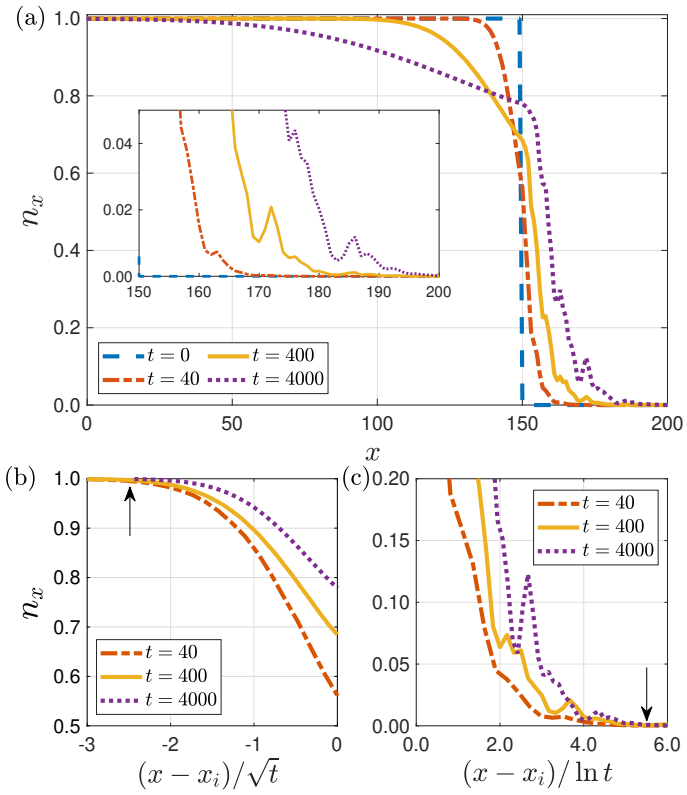

Figure 3.7: (a) Plot for density profile $n_x(t)$ as a function of x for different time snapshots for AAH lattice in the localized phase. (b) Density profile in the outer regime (sites with no probes), and (c) density profile for the outer regime.

3.2.6 Comparison of coherence plots as a justification for the phase coexistence

We observe that the inner front and outer front are significantly different concerning scaling, very clearly evidenced in the delocalized regime where both the speed of the front is remarkably different, and also the density profile in bulk has a lot of oscillatory features in the delocalized regime. This led us to hypothesize that the working principle for the dephasing probe might be deleting the off-diagonal correlations; for the sites at which the probes are attached. Thus we observed the time snapshots of the correlations for both the probe-connected section and the lattice section, which is free evolving. We present the results in this section. In our plots, we have chosen to show only the right half of the evolution, i.e. in

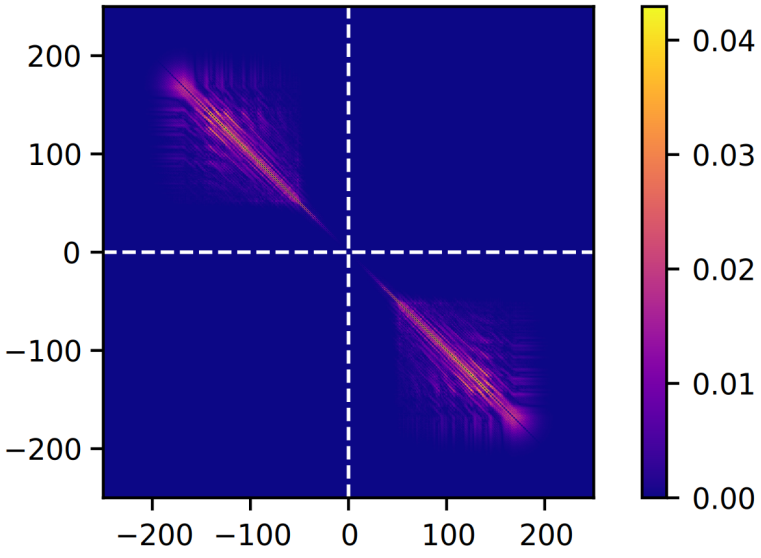

Figure 3.8: Plot of the absolute value of the correlations $\left\langle \hat{c}_i^\dagger \middle| \hat{c}_j \right\rangle$ after sufficient evolution in the density profile, we have divided the matrix into four sections, the top left and bottom right sections show correlations generated in the two halves of the lattice.

the correlation matrix, only the bottom right corner shows all the correlations in that region. A few points to notice, as shown in figure(3.6), is that the correlations in this region can be classified into four sections, the correlations $\left\langle \hat{c}_{outer}^\dagger \middle| \hat{c}_{outer} \right\rangle$ are the ones on the bottom right, the correlations $\left\langle \hat{c}_{inner}^\dagger \middle| \hat{c}_{inner} \right\rangle$ are the ones that are on the top left. A significant difference that comes up between the probed region and non-probed regions is the absence

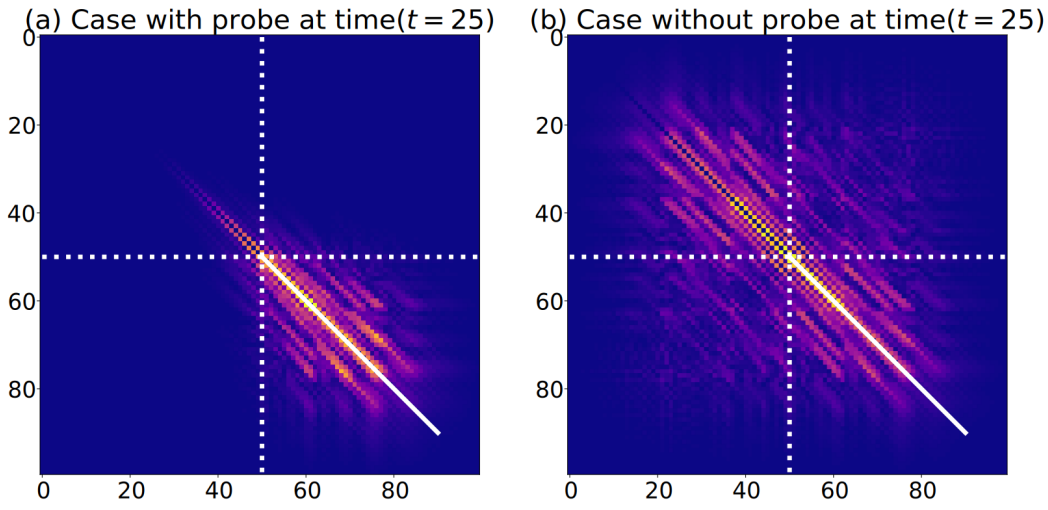

Figure 3.9: Here we compare the two correlation matrices the case with and without probe.

of off-diagonal correlations. In fig(3.9), we can see the effect that the extensive dephasing probe has on the coherence. The probes have killed all the off-diagonal coherences except the nearest neighbour ones. This is seen in the upper left corner of Fig (a) as compared to the non-probe case. This loss of coherences is what drives the diffusive nature as now the dynamics become classical in this regime, and this thus sets that the speed of the wavefront should scale as $\sqrt{t}$. This feature of the dephasing probe is independent of the nature of the underlying lattice, and as a result, we see that two phases coexist in our study.

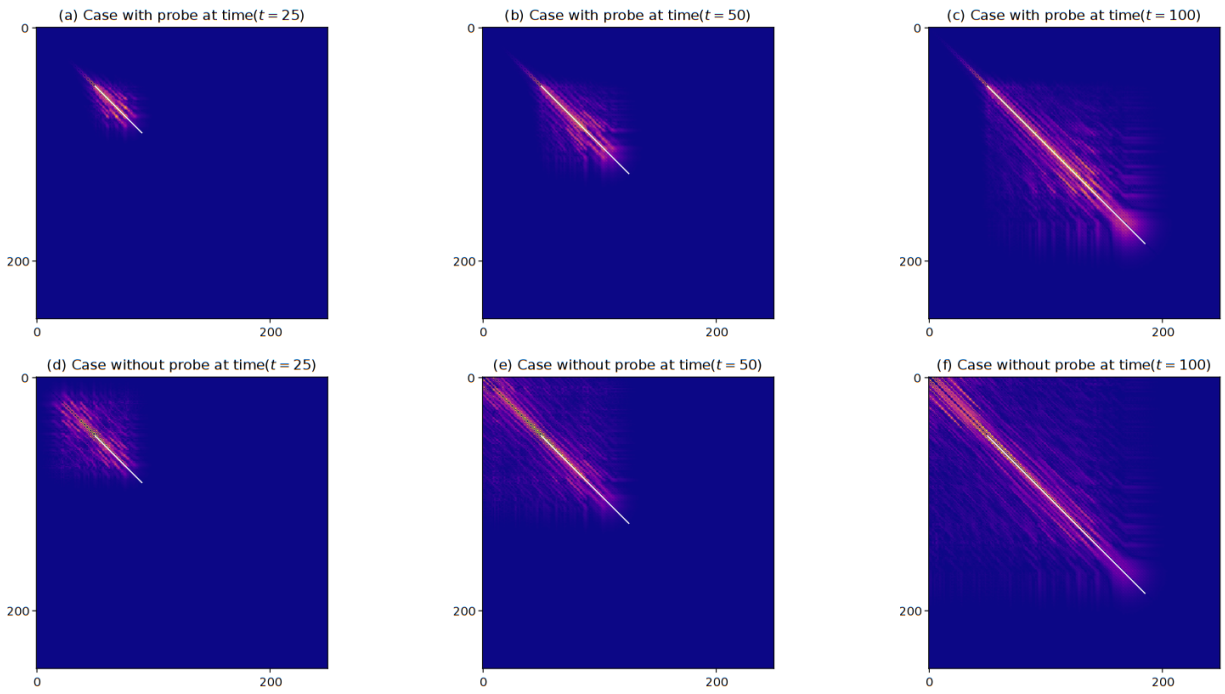

Figure 3.10: Plot of the absolute value of the correlations $\left\langle \hat{c}_i^\dagger \middle| \hat{c}_j \right\rangle$ after sufficient evolution in the density profile, we see the difference between the probe and the non-probe cases, as now coherences in the no-probe case are populating the upper left corner, but there is no coherences in the extensive probe case.

3.2.7 Case with $\sqrt{N}$ probes.

Now we take the same setup, but this time around, instead of connecting all the central sites, we connect $\sqrt{N_f}$ probes to the filled site. The dephasing probe in the extensive case was deleting all the off-diagonal coherence, but a $\sqrt{N}$ number of probes cannot achieve that. As a result, the unitary dynamics still survive in this case. Thus the features of two-phase coexistence is not realized in the $\sqrt{N}$ case. This can be seen in fig(3.11) where we have ten probes connected from site 0 to 100 at a regular interval but the $\left\langle \hat{c}_{inner}^\dagger \middle| \hat{c}_{inner} \right\rangle$ coherences still develop this in contrast to the extensive probe case where these coherences were completely deleted.

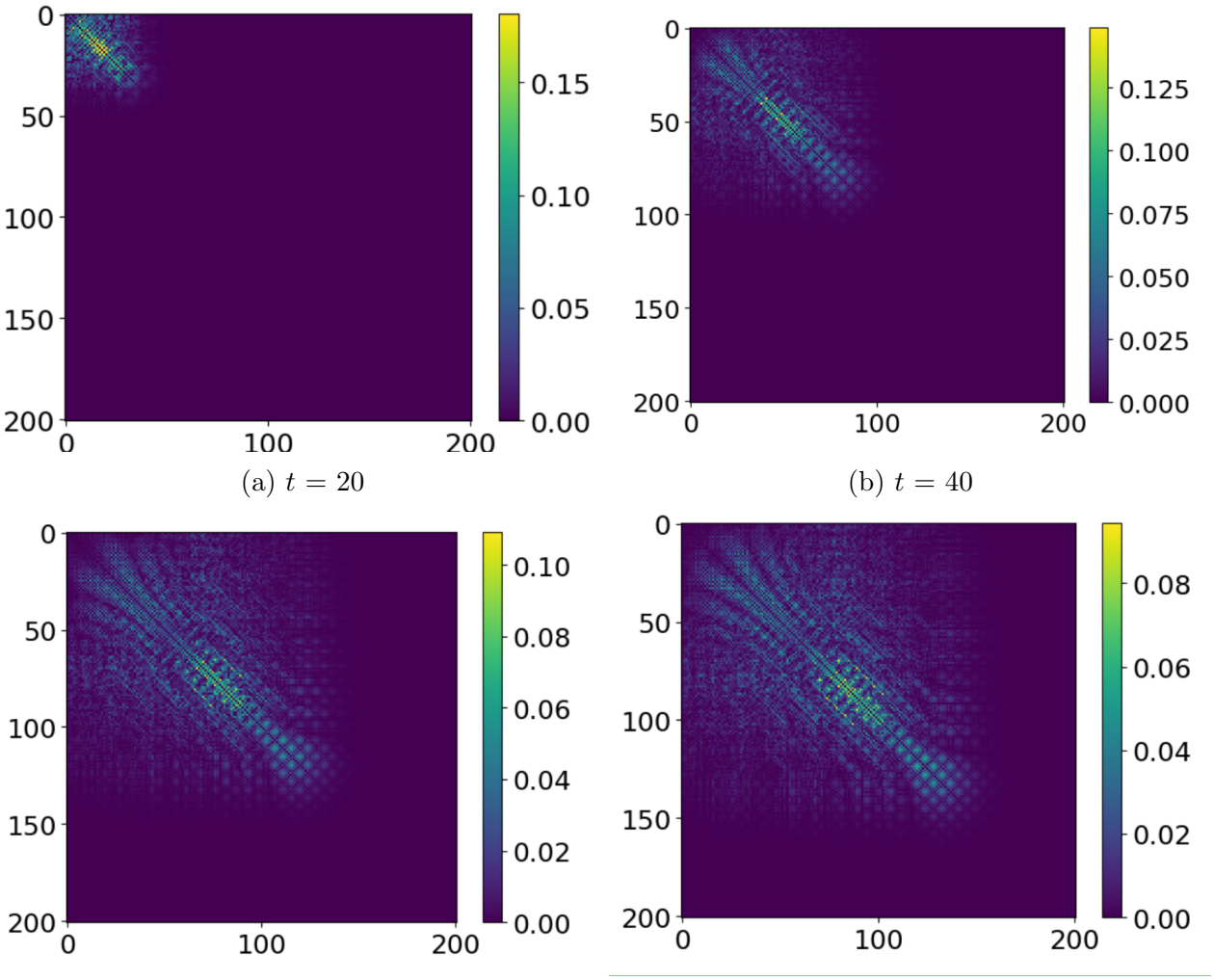

(a) $t = 20$

(b) $t = 40$

(c) $t = 60$

(d) $t = 80$

Figure 3.11: Coherence formation for the delocalised case when root n probes are connected at regular intervals in filled sites. We have 200 sites in total, with 100 sites filled initially and a total of 10 probes attached uniformly from site 0 to 100.

3.3 Summary and Outlook

In summary, we have seen the effect of a dephasing probe, which conserves the particle number through evolution but pumps energy into the system. Our observation has been that it can bring out dynamics only in the presence of sufficient initial coherence present in the system, as seen in the single probe case, which could not initiate dynamics independently unless the unitary dynamics have brought about enough coherence into the system. The single probe initiates a wave which has a velocity similar to the unitary dynamics, but because it only initiates after sufficient time has passed out till the central site is activated, there is a lag in both fronts. The extension of this problem we worked on was the extensive probe case, where we attached N_p probes to all the initially filled sites N_f. Our observations are encapsulated in the table below.

Phases with Probe		
Quasi-periodic Potential	Probeless	Behaviour with Probe
Clean Chain ($\lambda = 0$, $\alpha = 0$)	Ballistic	Ballistic and Diffusive
AAH Deloclaized ($\lambda = 0.5$, $\alpha = 0$)	Ballistic	Ballistic and Diffusive
AAH Critical ($\lambda = 1.0$, $\alpha = 0$)	Diffusive	Diffusive
AAH Localized ($\lambda = 1.1$, $\alpha = 0$)	Localized	Localized and Diffusive

Thus we see that irrespective of the nature of the underlying lattice; the extensive dephasing probe takes all the density wavefront velocities to a diffusive scaling. To understand how this happens, we studied the coherence features of the lattice. We showed how the dephasing probes kill all the coherence and thus bring about the classical feature of a diffusive wavefront. We also showed that $\sqrt{N}$ probes cannot kill the coherence; thus, the diffusive feature does not arise in this case. We want to extend the result to the GAAH model with a mobility edge and see how the dephasing probe behaves for that quasi-periodic model. We also have to show how the crossover from the $\sqrt{N}$ number of probes to the extensive probe regime affects the velocity scaling and determine whether there is a critical number of probes that can achieve the diffusive scaling.

Chapter 4

Conclusion

We set out to understand the open quantum system involving a quasi-periodic lattice coupled with a dephasing environment. Our results provided two important conclusions, the first being that there is a universal power law decay of the conductance in an AAH lattice with the increase in the strength of the dephasing probe, showing the effect of a single Büttiker probe on the steady-state transport properties. There is also an enhancement in conductance for the no-transport regime of the AAH model in a small lattice. The second conclusion deals with the dynamical evolution of the quasi-periodic lattice. The absence of a probe induces unitary dynamics in the closed system, thus reflecting the underlying property of the AAH model. It shows a ballistic transport for the delocalized regime, a diffusive transport in the critical regime and a ceasing of transportation in the localized regime. But adding an extensive dephasing probe universally takes transport in all phases of this quasi-periodic lattice to diffusive transport. The loss of off-diagonal correlations also shows that the probe has killed coherence, and thus the transport has moved from a quantum one to a classical one. We also showed that the extensive nature of the probe is essential in bringing out this phenomenon. It will be interesting to investigate the setup further to understand the emergence of diffusive properties in the presence of an extensive number of probes but placed randomly across the lattice or if the probe interactions are random. The effect of the sub-extensive number of probes is less explored in this thesis. This is an interesting problem to understand the transport properties. The final steady state of this setup is also worth studying, as how the system might thermalize differently for the different initial conditions. Various quasi-periodic models can also be studied including the Fibonacci model which provides super-diffusive and sub-diffusive phases.

Bibliography

[1] S. Aubry, G. André, Analyticity breaking and anderson localization in incommensurate lattices, Ann. Israel Phys. Soc 3 (133) (1980) 18.

[2] P. G. Harper, Single band motion of conduction electrons in a uniform magnetic field, Proceedings of the Physical Society. Section A 68 (10) (1955) 874.
URL https://iopscience.iop.org/article/10.1088/0370-1298/68/10/304

[3] A. M. Lacerda, J. Goold, G. T. Landi, Dephasing enhanced transport in boundary-driven quasiperiodic chains, Physical Review B 104 (17) (2021) 174203.
URL https://journals.aps.org/prb/pdf/10.1103/PhysRevB.104.174203

[4] M. Saha, B. P. Venkatesh, B. K. Agarwalla, Quantum transport in quasiperiodic lattice systems in the presence of büttiker probes, Physical Review B 105 (22) (2022) 224204.
URL https://journals.aps.org/prb/pdf/10.1103/PhysRevB.105.224204

[5] V. K. Varma, C. de Mulatier, M. Žnidarič, Fractality in nonequilibrium steady states of quasiperiodic systems, Phys. Rev. E 96 (2017) 032130. doi:10.1103/PhysRevE.96.032130.
URL https://link.aps.org/doi/10.1103/PhysRevE.96.032130

[6] J. Schwinger, Brownian motion of a quantum oscillator, Journal of Mathematical Physics 2 (3) (1961) 407–432.
URL https://aip.scitation.org/doi/pdf/10.1063/1.1703727

[7] H. Haug, A.-P. Jauho, et al., Quantum kinetics in transport and optics of semiconductors, Vol. 2, Springer, 2008.
URL https://doi.org/10.1007/978-3-540-73564-9

[8] J. Rammer, H. Smith, Quantum field-theoretical methods in transport theory of metals,

Rev. Mod. Phys. 58 (1986) 323–359. doi:10.1103/RevModPhys.58.323.
URL https://link.aps.org/doi/10.1103/RevModPhys.58.323

[9] J.-S. Wang, B. K. Agarwalla, H. Li, J. Thingna, Nonequilibrium greens function method for quantum thermal transport, Frontiers of Physics 9 (2014) 673–697.
URL https://doi.org/10.1007/s11467-013-0340-x

[10] H.-P. Breuer, F. Petruccione, et al., The theory of open quantum systems, Oxford University Press on Demand, 2002.

[11] H. Carmichael, Statistical methods in quantum optics 1: master equations and Fokker-Planck equations, Vol. 1, Springer Science & Business Media, 1999.
URL https://doi.org/10.1007/978-3-662-03875-8

[12] E. B. Davies, Quantum theory of open systems, Academic Press, 1976.

[13] R. Alicki, K. Lendi, Quantum dynamical semigroups and applications, Vol. 717, Springer, 2007.
URL https://doi.org/10.1007/3-540-70861-8

[14] C. Gardiner, P. Zoller, P. Zoller, Quantum noise: a handbook of Markovian and non-Markovian quantum stochastic methods with applications to quantum optics, Springer Science & Business Media, 2004.

[15] P. W. Anderson, Absence of diffusion in certain random lattices, Phys. Rev. 109 (1958) 1492–1505. doi:10.1103/PhysRev.109.1492.
URL https://link.aps.org/doi/10.1103/PhysRev.109.1492

[16] A. Purkayastha, S. Sanyal, A. Dhar, M. Kulkarni, Anomalous transport in the aubry-andré-harper model in isolated and open systems, Physical Review B 97 (17) (2018) 174206.
URL https://journals.aps.org/prb/pdf/10.1103/PhysRevB.97.174206

[17] A. Dhar, D. Sen, Nonequilibrium green's function formalism and the problem of bound states, Phys. Rev. B 73 (2006) 085119. doi:10.1103/PhysRevB.73.085119.
URL https://link.aps.org/doi/10.1103/PhysRevB.73.085119

[18] M. V. Medvedyeva, T. c. v. Prosen, M. Žnidarič, Influence of dephasing on many-body localization, Phys. Rev. B 93 (2016) 094205. doi:10.1103/PhysRevB.93.094205.
URL https://link.aps.org/doi/10.1103/PhysRevB.93.094205

[19] A. Lahiri, K. Gharavi, J. Baugh, B. Muralidharan, Nonequilibrium green's function study of magnetoconductance features and oscillations in clean and disordered nanowires, Phys. Rev. B 98 (2018) 125417. doi:10.1103/PhysRevB.98.125417.
URL https://link.aps.org/doi/10.1103/PhysRevB.98.125417

[20] P. E. Dolgirev, J. Marino, D. Sels, E. Demler, Non-gaussian correlations imprinted by local dephasing in fermionic wires, Physical Review B 102 (10) (2020) 100301.
URL https://journals.aps.org/prb/pdf/10.1103/PhysRevB.102.100301

[21] J. L. dAmato, H. M. Pastawski, Conductance of a disordered linear chain including inelastic scattering events, Physical Review B 41 (11) (1990) 7411.
URL https://journals.aps.org/prb/pdf/10.1103/PhysRevB.41.7411

[22] H. Haken, G. Strobl, An exactly solvable model for coherent and incoherent exciton motion, Zeitschrift für Physik A Hadrons and nuclei 262 (2) (1973) 135–148.
URL https://doi.org/10.1007/BF01399723

[23] X. Turkeshi, M. Schiró, Diffusion and thermalization in a boundary-driven dephasing model, Physical Review B 104 (14) (2021) 144301.
URL https://journals.aps.org/prb/pdf/10.1103/PhysRevB.104.144301

[24] S. R. Taylor, A. Scardicchio, Subdiffusion in a one-dimensional anderson insulator with random dephasing: Finite-size scaling, griffiths effects, and possible implications for many-body localization, Phys. Rev. B 103 (2021) 184202. doi:10.1103/PhysRevB.103.184202.
URL https://link.aps.org/doi/10.1103/PhysRevB.103.184202

[25] A. Dorda, M. Nuss, W. von der Linden, E. Arrigoni, Auxiliary master equation approach to nonequilibrium correlated impurities, Phys. Rev. B 89 (2014) 165105. doi:10.1103/PhysRevB.89.165105.
URL https://link.aps.org/doi/10.1103/PhysRevB.89.165105

[26] E. Süli, D. F. Mayers, An introduction to numerical analysis, Cambridge university press, 2003.

[27] G. B. Arfken, H. J. Weber, Mathematical methods for physicists (1999).